Electronic structure and stability of hyperstoichiometric UO_{2+x} under pressure

Jianwei Wang,* Rodney C. Ewing, and Udo Becker
University of Michigan, Department of Earth and Environmental Sciences, Ann Arbor, Michigan 48109-1005, USA
(Received 23 November 2011; revised manuscript received 22 February 2013; published 15 July 2013)

Electronic-Structure and high-pressure phase transitions of stoichiometric uranium dioxide (UO_2) and hyperstoichiometric $UO_{2.03}$ were investigated using first-principles calculations. Density functional theory calculations using the generalized gradient approximation and the projector-augmented wave method with the on-site Coulomb repulsive interactions were applied in order to reasonably calculate the equilibrium volume, total and partial density of states, band gap of UO_{2+x}, and energetics of the high-pressure phase transitions. Structure optimizations were completed with and without the Hubbard U-ramping method separately. The U-ramping method was intended to remove the metastable states of the $5f$ electrons of both stoichiometric and hyperstoichiometric UO_{2+x}. Using the Hubbard U parameters ($U = 3.8$, $J = 0.4$), whose values are based on the experimental band gap width of 2.1 eV as a reference, the calculated cell parameter for the stoichiometric UO_2 with cubic fluorite structure is about 1% greater than the experimental unit cell parameter; in contrast, it is about 1% smaller than the experimental value without the on-site Coulomb repulsive interactions. For hyperstoichiometric $UO_{2.03}$ with the cubic fluorite structure, the interstitial oxygen at the octahedral interstitial site induces new bands at the top of the band gap of the stoichiometric UO_2, similar to those of the high-pressure phase with orthorhombic cotunnite structure. The orbitals associated with the charge transfers to the interstitial oxygen in hyperstoichiometric $UO_{2.03}$ are partially delocalized and partially localized in both the cubic fluorite structure and orthorhombic cotunnite structure. The energy required for the incorporation of an interstitial O atom is 0.3 eV higher for the orthorhombic phase than for the cubic phase at ambient pressure and increases to 0.5 eV at 10 GPa. The calculated transition pressures from the cubic to the orthorhombic structure are 18 and 27 GPa for UO_2 and $UO_{2.03}$, respectively. The dramatic increase in the calculated transition pressure for the hyperstoichiometric UO_2 is related to structural incompatibility of the interstitial oxygen in the cotunnite structure (high-pressure phase), which is less in the case of the fluorite structure. These results suggest that experimentally determined pressure values for the phase transition can be significantly affected by small compositional deviations off the ideal stoichiometric UO_2. Comparisons of the results using the U-ramping method and without using the U-ramping method suggest that the electronic metastability of UO_2 affects the calculated total energy and electronic structure and could lead to a different local defect configuration for the hyperstoichiometric orthorhombic phase. However, the metastability has a negligible effect on the calculated phase transition pressure.

DOI: 10.1103/PhysRevB.88.024109 PACS number(s): 61.72.−y, 64.70.K−, 71.15.Mb, 81.40.Vw

I. INTRODUCTION

Uranium dioxide (UO_2) is the most common nuclear fuel, accounting for approximately 95% of spent nuclear fuel from commercial reactors.[1] Of special interest is the behavior of UO_2 under high temperatures and high pressures and under the extreme environment of a high radiation field. At present, it is very difficult to reliably predict the fundamental properties that affect the performance of UO_2 in the reactor environment or in a reactor accident.[2–6] Experimentally, it is a great challenge to characterize each of the many processes under the operating conditions in a reactor and to isolate the specific contributions of each process to the changes in the properties of UO_2.[7] In addition, the restricted handling of highly radioactive materials due to safety considerations makes experiments with real fuel costly and time consuming. For this reason, computational modeling and simulations have been used as an advantage and applied to the study of UO_2. These studies have significantly improved the understanding of the electronic structure,[8–19] defects,[8,9,12,20–25] thermodynamics,[26] thermal properties,[27–29] and diffusion properties[8,30–34] of UO_2. Among many issues considered by theoretical treatments of UO_2 are the localization and delocalization of unpaired $5f$ electrons, spin-orbit coupling, relativistic effects, spin ordering, orbital anisotropy of U, and, more recently, electronic metastability involving $5f$ electrons and charged defects in density functional theory (DFT) + U calculations.[9,13,35–37]

Still, an appropriate electronic structure description of UO_2 for a full range of conditions has not been developed. For instance, while the local density approximation (LDA), with an appropriate Hubbard U parameter, calculates the electronic band gap correctly,[12] the predicted phase transition pressure from the fluorite structure to the cotunnite structure is 7.8 GPa,[14] which is too low compared with experimental observations in the range of 29–42 GPa.[38,39] With generalized gradient approximation (GGA) + U, the predicted phase transition pressure is improved (on the order of 20 GPa)[12] but is still below the observed values.[38,39] In addition, there are large discrepancies in the defect formation energies for each type of defects among different theoretical calculations.[12,13,20,21,23,24] One reason for these discrepancies has been identified to be multiple metastable electronic states of UO_2, which prevent the system from reaching the true electronic ground state because of the use of the DFT + U approximation.[20] Multiple metastable electronic states have been demonstrated for the perfect and defect UO_2 with the fluorite structure[13,20] and also for metals and other compounds such as Ce,[40] PuO_2,[41] and PrO_2.[42] A recent improvement to determine the ground state of actinide oxides within a DFT + U calculation is to employ the proposed density matrix controlling scheme.[13] However,

only initial diagonal occupation matrices are imposed, and each of the individual U atoms is not treated separately. For a larger system with defects, each U atom could have a different density matrix. It is not computationally practical to enumerate all the possible initial electronic configurations, not even to mention the off-diagonal elements of the occupation matrices. Other methods to overcome the metastability problem have been proposed, including the Hubbard U-ramping method,[35] the quasi-annealing procedure,[36] a guessing procedure,[37] and by simply trying multiple calculations for a given system.[8] To this time, there has not been a simple and computationally less demanding approach that guarantees a UO_2 system to converge to its true electronic ground state. In addition, confirming the true electronic ground state for a given system is challenging because the current methods are intended to find the lowest energy possible within a given method, which does not need to be the true ground state. The discrepancies among different calculations of same properties (e.g., defect formation energies)[20] and between theoretical calculations and experimental observations[12,14] emphasize the need to benchmark theoretical calculations with experimental data.

The stoichiometry of UO_{2+x} varies depending on temperature and oxygen pressure,[43–49] and the composition is formulated as UO_{2+x} (for $x < 0$: oxygen content deficiency, i.e., hypostoichiometric; for $x > 0$: oxygen excess, i.e., hyperstoichiometric). In experiments, the U/O ratio can be as high as 2.24 for UO_{2+x} with the cubic fluorite structure, very close to the ratio of the U_4O_9 phase.[43] In nuclear reactors, "x" typically varies in a smaller range (0.0–0.1).[6] Thus, UO_{2+x} with different thermal histories and syntheses over a range of oxygen fugacities is expected to have different x values. The effect of x on the properties of UO_2, such as diffusion parameters of the O and U atoms, has been widely documented.[6,7,50–53] However, the effect of the excess oxygen on other fundamental properties of UO_{2+x}, such as the electronic structure and phase transition pressure of UO_2, has not been fully investigated. In order for experimental observations to better serve as benchmarks for the theoretical treatment of UO_{2+x}, the effect of x on the properties of UO_2 must be fully understood. The reported experimentally determined phase transition pressures of UO_2 from the cubic fluorite structure ($Fm\bar{3}m$) to the orthorhombic cotunnite structure ($Pnma$) vary from 29 GPa[39] to 42 GPa.[38] Although the cause for such a large difference is not clear, a deviation of the chemical composition from the ideal stoichiometry has not been investigated. In addition to the oxygen stoichiometry, other deviations from the ideal chemical composition are also expected to affect the phase behavior in temperature-pressure space. For instance, for a natural sample of UO_2 with ~8 weight percent (wt%) PbO, the $Fm\bar{3}m$ to the $Pnma$ phase transition was not observed, but two new phase transitions were detected.[54]

In this paper, the electronic structures and stabilities of stoichiometric UO_2 and hyperstoichiometric UO_{2+x} ($x = 0.03$, or 0.2 wt%) as a function of pressure have been calculated using first-principles methods. The effect of x on the crystal structure, electronic structure, and phase transition pressure is evaluated by considering local defect structures, defect bands, charge transfer around the oxygen interstitial, and energetics of interstitial oxygen incorporation into the structures. The trend of the effect on the properties instead of the calculated absolute values will be the focus. Comparisons between the results using the U-ramping method and without using the U-ramping method provide important insights on how the electronic metastability of UO_2 affects the calculated electronic structure, defect configuration, and high pressure phase transition.

II. METHODS AND CALCULATIONS

A. DFT calculations

Quantum-mechanical calculations were performed using the DFT framework and plane wave basis sets as implemented in the Vienna *Ab initio* Simulation Package (VASP).[55] The projector-augmented wave (PAW) method[56] and exchange correlation as parameterized by the Perdew–Wang 91 functional[57,58] were applied in the GGA-PAW.[59] The potentials supplied by VASP (optimized for the PAW approach) were used in the calculations. The 5*f, 6s, 6p, 6d,* and *7s* electrons of U were treated as valence electrons (total of 14 valence electrons), and the core electrons (with [Xe, $5d, 4f$] configuration) were approximated by using pseudopotentials. For O, the core has a [He] configuration, and the remaining six electrons were treated as valence electrons. The on-site Coulomb interactions with the simplified rotational invariant approach (the Dudarev approach),[60] fully relativistic calculations for the core electrons (represented as pseudopotential), and scalar relativistic approximations for the valence electrons[61,62] were employed to reasonably account for the relativistic effects and electron correlation of the $5f$ electrons in UO_2.

The calculations were performed using a 12-atom cell for stoichiometric UO_2 and a 97-atom supercell ($2 \times 2 \times 2$ unit cells of UO_2 with one extra oxygen) for hyperstoichiometric $UO_{2.03}$. The energy cutoff for the plane wave basis set was 520.00 eV (or 38.2 Ry) for all calculations. The Monkhorst–Pack scheme for the integration in the Brillouin zone was adopted. The number of k-points was tested for energy convergence of each system. For the 12-atom cell calculations, $8 \times 8 \times 8$ and $8 \times 12 \times 8$ k-point grids were used for the fluorite and the cotunnite structures, respectively. For the 97-atom cell calculations, $3 \times 3 \times 3$ and $3 \times 5 \times 3$ k-point grids were used for the two structure types, respectively. The ground state of UO_2 with the fluorite structure has a $3k$ antiferromagnetic (AFM) spin configuration, where the magnetic moments of U atoms are oriented along ⟨111⟩, which is supported by a recent experimental study.[63] However, a $1k$ AFM ordering, where the moments of U atoms are oriented along ⟨001⟩, is a good approximation to the $3k$ ordering, as demonstrated in a recent study with a difference in total energy of ~2.4 meV/12-atom cell between the two magnetic configurations.[20] For the cotunnite structure with $Pnma$ symmetry, calculations (details in the Results and Discussion section) show that the AFM structure with the magnetic moments of U atoms in the ⟨100⟩ directions has the lowest energy.

Thus, in this paper, the $1k$ AFM order was adopted for both structures, and collinear magnetic calculations were performed for simplicity. The results based on the $1k$ order are not expected to strongly affect the conclusions presented here. For the stoichiometric UO_2 calculations, symmetry was not applied for both structures in order to better compare

with the calculations on hyperstoichiometric $UO_{2.03}$, where the same spin configuration was used without symmetry. For the AFM configuration of the fluorite structure, without constraints on the computational cell shape, the cubic cell is slightly distorted, and the distortion of the three lattice vectors is low (*i.e.*, less than 1%). The energy difference is ∼10 meV/12-atom cell between with and without allowing lattice distortion, which is relatively small compared with the energy differences between different compositions and structures that are discussed in the later sections of this paper. Therefore, all calculations were performed without allowing a change in the computational cell shape (i.e., the angles). Previous studies have shown that spin-orbit coupling in UO_2 is quite strong in terms of total energy.[12,64,65] However, it has been demonstrated that inclusion of spin-orbit coupling only has a limited effect on the bulk and one-electron properties of UO_2.[12,65–70] As a recent article[70] points out, it has been numerically found[65,66] and physically analyzed[67,68] that inclusion of the spin-orbit coupling has little effect on the bulk and one-electron properties of UO_2. For instance, calculations of UO_2 with the spin-orbit coupling show that the band gap decreases by only 0.06 eV and that the spin-orbit coupling is a minor perturbation.[69] Previous calculations for PuO_2, a similar system with unpaired $5f$ electrons, show that the inclusion of the spin-orbit coupling will increase the equilibrium lattice constant by only 0.7% and the bulk modulus by about 0.5 GPa.[70] As demonstrated in a recent paper, the lattice constant of UO_2 is predicted to be within 1% difference between with/without spin-orbit coupling.[12] Although the spin-orbit coupling is strong, the contribution to the total energy is not very sensitive to a change of the lattice constant. This is probably because $5f$ electrons in UO_2 are largely localized and the spin-orbit coupling is not strongly affected by a change of the bond distances in UO_2. Thus, spin-orbit coupling is not included in the present calculations due to complications involving the spin-orbit coupling of the $5f$ electrons and the computational effort required for what would be a small improvement in the accuracy on the calculated properties.

B. Defect models of $UO_{2.03}$ with fluorite and cotunnite structures

The defect structures of hyperstoichiometric UO_{2+x} with the fluorite structure have been extensively studied experimentally and theoretically.[9,22,33,71–74] For low x values, isolated point defects are expected. As the x value increases, oxygen defects tend to form clusters and become progressively complex at higher x values.[22,33,71] In most cases, the majority of defects are oxygen interstitials rather than uranium vacancies.[72] In this study, one extra oxygen atom was added in the structure with 96 atoms ($2 \times 2 \times 2$ supercell), resulting in 97 atoms in the supercell (32 U and 65 O) with $x = 65/32 - 2 \approx 0.03$. At this low x value, the oxygen atom tends to form a point defect in the fluorite structure. Therefore, the extra oxygen atom was inserted at the empty interstitial position, formed by the uranium octahedron [Fig. 1(a)]. For the cotunnite structure, no empty interstitial site exists in the lattice. An extra oxygen was inserted at a similar location as that in the fluorite structure [Fig. 1(b)].

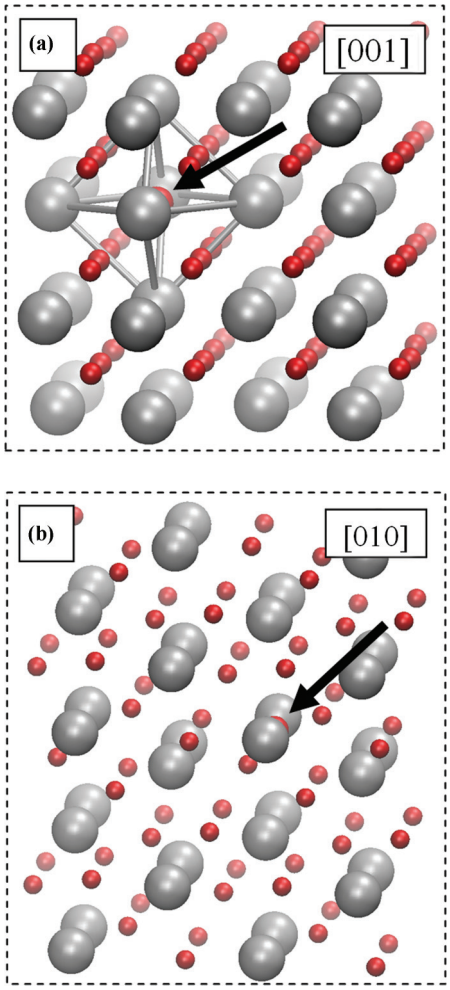

FIG. 1. (Color online) Structures of UO_2. (a) Fluorite-like cubic, $Fm\bar{3}m$, projected along [001]; (b) cotunnite-like orthorhombic, $Pnma$, along [010]. The arrows point to the interstitial O atoms. In panel (a), the thick lines connecting atoms highlight the U octahedron, inside which is the interstitial site.

C. Electronic metastability of $5f$ electrons in UO_{2+x}

Metastable electronic states of cubic fluorite UO_2 have been documented,[13,35–37] and the lowest energy state may be obtained by controlling the initial occupation matrices of the U $5f$ electrons, by allowing $5f$ electrons to break the cubic symmetry,[13] by using a quasiannealing method,[36] or by using a $U-$ramping method.[35] In this study, two procedures were used to optimize the structures separately. In the conventional procedure, the initial occupation matrix for U was not controlled, but the occupation matrix was checked and the system symmetry was switched off, which would allow the system to reach its lower energy states.[13] The unpaired $5f$ electrons were initially averaged to the diagonal elements of the occupation matrices, and the off-diagonal elements were set to zero for each U atom. For the cubic fluorite structure, the final converged structure has an occupation matrix of a U atom as shown in Table I, and the matrix elements are similar to those of the U occupation matrix of the lowest energy states found from an earlier study, just ∼10 meV/12 atoms above the lowest state.[13] The density matrix elements are close to 0 or 1. Although the

TABLE I. The on-site density occupation matrix of the 5f electrons of a uranium in UO_2 with cubic fluorite structure.

			Spin component 1			
0.0420	0.0000	0.0084	0.0000	0.0000	0.0000	0.0000
0.0000	0.1372	0.0000	0.0000	0.0000	0.0000	0.0000
0.0084	0.0000	0.0377	0.0000	0.0000	0.0000	0.0000
0.0000	0.0000	0.0000	0.9278	0.0000	0.2198	0.0000
0.0000	0.0000	0.0000	0.0000	0.1901	0.0000	−0.3516
0.0000	0.0000	0.0000	0.2198	0.0000	0.0880	0.0000
0.0000	0.0000	0.0000	0.0000	−0.3516	0.0000	0.8258
			Spin component 2			
0.0338	0.0000	0.0043	0.0000	0.0000	0.0000	0.0000
0.0000	0.1186	0.0000	0.0000	0.0000	0.0000	0.0000
0.0043	0.0000	0.0315	0.0000	0.0000	0.0000	0.0000
0.0000	0.0000	0.0000	0.0376	0.0000	−0.0012	0.0000
0.0000	0.0000	0.0000	0.0000	0.0317	0.0000	−0.0058
0.0000	0.0000	0.0000	−0.0012	0.0000	0.0263	0.0000
0.0000	0.0000	0.0000	0.0000	−0.0058	0.0000	0.0323
			With the U-ramping method			
			Spin component 1			
0.2370	−0.0042	0.1284	0.2280	−0.1098	−0.2373	−0.0712
−0.0042	0.1371	−0.0081	−0.0161	0.0145	0.0222	−0.0077
0.1284	−0.0081	0.1167	0.1106	−0.0823	−0.1867	−0.0058
0.2280	−0.0161	0.1106	0.6086	−0.0214	−0.0105	−0.3670
−0.1098	0.0145	−0.0823	−0.0214	0.1444	0.2526	−0.0908
−0.2373	0.0222	−0.1867	−0.0105	0.2526	0.6326	−0.2170
−0.0712	−0.0077	−0.0058	−0.367	−0.0908	−0.217	0.4017
			Spin component 2			
0.0356	0.0091	0.0053	−0.0075	−0.0014	0.0041	−0.0014
0.0091	0.1148	0.0016	−0.0015	0.0026	−0.0032	−0.0067
0.0053	0.0016	0.0303	−0.0016	−0.0006	0.0006	0.0001
−0.0075	−0.0015	−0.0016	0.0407	0.0002	−0.0009	0.0101
−0.0014	0.0026	−0.0006	0.0002	0.0309	−0.001	−0.0053
0.0041	−0.0032	0.0006	−0.0009	−0.001	0.0253	0.0036
−0.0014	−0.0067	0.0001	0.0101	−0.0053	0.0036	0.0340

lowest energy state or the ground state was not obtained in the calculation, the error in the total energy is estimated to be around 10 meV per 12 atoms. For hyperstoichiometric $UO_{2.03}$ with the cubic fluorite structure, the final converged density matrix is shown in Table II, similar to that of the ground state for one of the uranium atoms, although the simplified rotationally invariant Dudarev approach[60] was used in this study compared with the rotationally invariant Liechtenstein approach[75] used in the previous study.[20] The small differences in the values of the matrix elements may be caused by the different approaches to treat the on-site Coulomb interactions and other computational details, including the Hubbard U parameters and computational cell and symmetry constraints. It is interesting to note that the hyperstoichiometry causes the density matrix elements to be less close to 0 or 1 (Tables I and II).

In order to check how high the energies of the as-converged states (i.e., using the first procedure) are with respect to their respective ground states and, more importantly, the effect of metastability on estimating the phase transition pressure, a second procedure using the Hubbard U-ramping method[35] was used to converge all the systems to their ground states. The reason for choosing the U-ramping method is its relative ease of use with the standard VASP code. In this second procedure, the Hubbard U term is adiabatically switched on with an initial value $U = 0.0$. At each step of the subsequent optimizations, the Hubbard U term is increased by a small value (e.g., 0.1 eV) until all the bands are integrally occupied. Then, the U term is increased to the desired value. The charge density and wave function are read from the previous step. As shown in Fig. 2, the number of fractional bands decreases as the Hubbard U is ramped up from 0.0. The number of the steps to obtain the insulating state is highly dependent on the initial structure, which is often less for stoichiometric UO_2 structures in the $1 \times 1 \times 1$ supercell [Fig. 2(a)] than for the hyperstoichiometric $UO_{2.03}$ in the $2 \times 2 \times 2$ supercell [Fig. 2(b)]. The purpose of the U-ramping procedure is to obtain such a charge density and wave function that are expected to lead the system to its low-energy state, hopefully the ground state. The converged density matrices are quantitatively different from those that result without using the U-ramping method (Tables I and II). More elements of the density matrices have nonzero values, in contrast to those without using the U-ramping method. The calculated energies show that, for the fluorite structure, the

TABLE II. The on-site density occupation matrix of the U 5f electrons of a uranium in $UO_{2.03}$ with cubic fluorite structure.

			Spin component 1			
0.4783	0.0000	0.4615	−0.0822	0.0000	−0.0316	0.0000
0.0000	0.1392	0.0000	0.0000	0.0034	0.0000	−0.0053
0.4615	0.0000	0.5145	−0.0842	0.0000	−0.0352	0.0000
−0.0822	0.0000	−0.0842	0.0702	0.0000	0.0078	0.0000
0.0000	0.0034	0.0000	0.0000	0.7024	0.0000	−0.4249
−0.0316	0.0000	−0.0352	0.0078	0.0000	0.0343	0.0000
0.0000	−0.0053	0.0000	0.0000	−0.4249	0.0000	0.3097
			Spin component 2			
0.0319	0.0000	0.0044	0.0000	0.0000	0.0001	0.0000
0.0000	0.1182	0.0000	0.0000	0.0003	0.0000	−0.0025
0.0044	0.0000	0.0297	0.0009	0.0000	−0.0006	0.0000
0.0000	0.0000	0.0009	0.0400	0.0000	0.0016	0.0000
0.0000	0.0003	0.0000	0.0000	0.0295	0.0000	−0.0047
0.0001	0.0000	−0.0006	0.0016	0.0000	0.0263	0.0000
0.0000	−0.0025	0.0000	0.0000	−0.0047	0.0000	0.0373
			With the U-ramping method			
			Spin component 1			
0.4409	−0.0022	−0.1971	−0.0111	0.1750	0.0106	0.3829
−0.0022	0.1220	0.0018	0.0101	−0.0075	−0.0015	0.0000
−0.1971	0.0018	0.6170	−0.0046	0.3768	−0.0161	−0.1605
−0.0111	0.0101	−0.0046	0.0574	−0.0202	−0.0002	−0.0110
0.1750	−0.0075	0.3768	−0.0202	0.5913	−0.0063	0.1961
0.0106	−0.0015	−0.0161	−0.0002	−0.0063	0.0310	0.0094
0.3829	0.0000	−0.1605	−0.0110	0.1961	0.0094	0.4085
			Spin component 2			
0.0333	0.0003	0.0051	0.0005	−0.0030	−0.0003	−0.0002
0.0003	0.1038	0.0018	0.0068	−0.0017	−0.0012	0.0017
0.0051	0.0018	0.0253	0.0006	−0.0054	0.0002	0.0013
0.0005	0.0068	0.0006	0.0455	−0.0006	−0.0006	0.0012
−0.0030	−0.0017	−0.0054	−0.0006	0.0260	−0.0001	−0.0045
−0.0003	−0.0012	0.0002	−0.0006	−0.0001	0.0243	0.0008
−0.0002	0.0017	0.0013	0.0012	−0.0045	0.0008	0.0328

as-converged states are at most 0.08 eV/12-atom cell above the ground state for UO_2 and at most 0.16 eV/12-atom cell for $UO_{2.03}$. For the cotunnite structure, the as-converged states are at most 0.04 and 0.07 eV/12-atom cell for the respective compositions. The results suggest the U-ramping method indeed leads to lower energy states of the systems. Thus, all the reported values are based on the U-ramping method unless explicitly mentioned otherwise. Details of the effect of the electronic metastability on the electronic structure, defect structure, and phase transition pressure are discussed in the following sections.

III. RESULTS AND DISCUSSION

A. Properties of stoichiometric UO_2

For stoichiometric UO_2 with the cubic fluorite structure, conventional DFT schemes (e.g., LDA, GGA) predict a metallic electronic ground state, which is inconsistent with the experimental observation of an insulating state of the material.[76] In order to reproduce the band gap of UO_2, the on-site Coulomb repulsion for the U 5f electrons is introduced by adding the Hubbard U term to the DFT functional. Different Hubbard U values have been used in the literature.[8,12,22,35] In some recent DFT calculations, $U = 4.5$ eV and $J = 0.51$ eV have been used,[8,22,35] which are based on experimental measurements.[18] Since the Hubbard U term is originally used to correct the insulating band gap, in this study, an observed band gap width of UO_2 is needed to estimate the Hubbard U parameters. The $5f^2$-$5f^16d$ transition of ∼2.1 eV derived from a reflectivity measurement was used for this purpose.[77] The electron density of states was calculated as in the literature for UO_2[15,78,79] at the equilibrium volume for a series of different Hubbard U parameters. Upon increasing the U and J, the energy gap increases as expected. The optimized parameters for U and J are $U = 3.8$ and $J = 0.4$ with an energy gap of 1.9 eV, without using the Hubbard U-ramping method, or 2.2 eV using the ramping method, which is close to 2.1 eV, the experimental value.[77] Although it is difficult to justify the comparison between the $5f^2$-$5f^16d$ transition from the experiment and the intra-5f band gap from the DFT calculation, for simplicity, the experimental band gap was used here as a reference value to estimate the Hubbard U values. In Fig. 3, the total density of states [Fig. 3(a)] is plotted along with the partial densities of states for U [Fig. 3(b)] and O [Fig. 3(c)]. As the figures illustrate, at the top of the valence bands are mainly U 5f states, with a small contribution from the O 2p

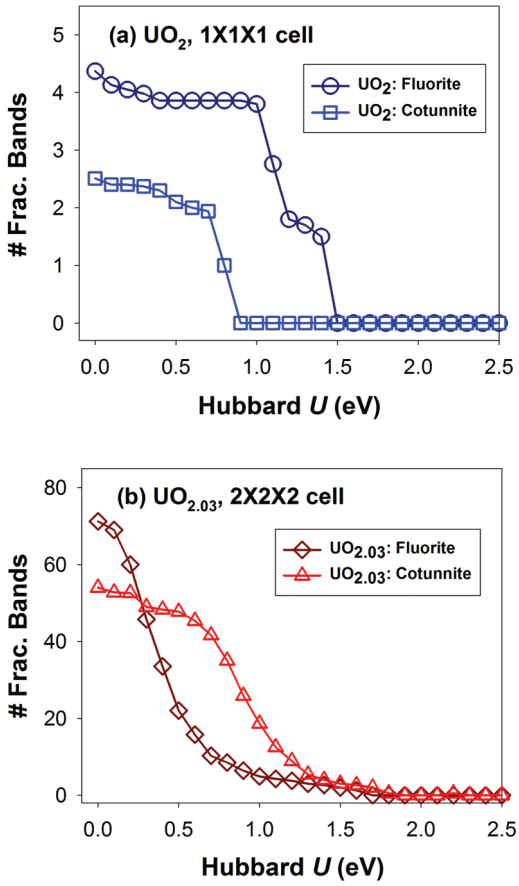

FIG. 2. (Color online) Number of fractional bands as a function of the Hubbard U parameter for the fluorite and cotunnite structures. (a) UO_2 in the $1 \times 1 \times 1$ cell with 12 atoms. (b) $UO_{2.03}$ in the $2 \times 2 \times 2$ cell with 97 atoms.

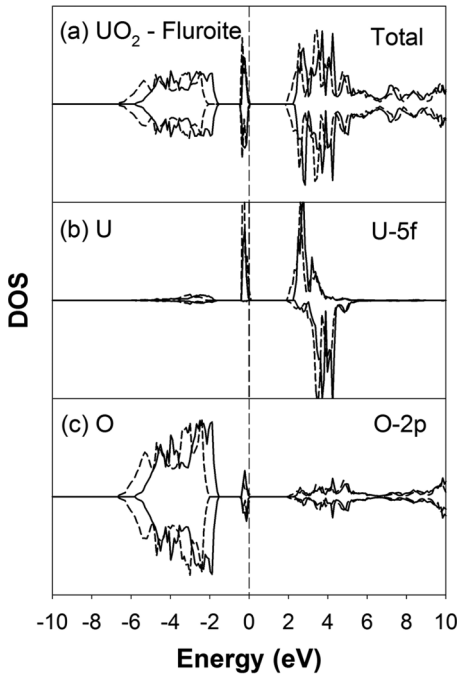

FIG. 3. Electron density of states (DOS) of UO_2 with the fluorite structure with (solid lines) and without (dashed lines) the Hubbard U-ramping method. (a) The total density of states. (b) Partial density of states of an up-spin U atom in UO_2. (c) Partial density of states of an O atom in UO_2. The vertical dashed line is the location of the Fermi level. Each DOS is arbitrarily rescaled for clarity.

states, in agreement with a photoemission study.[80] Below the Fermi level, in the range of -1.6 to approximately -5.8 eV, are mainly electrons from O $2p$ [Fig. 3(c)], with only a small contribution from U $6d$ and $5f$ electrons, consistent with the experimental observation[80] and previous theoretical calculations.[15,17,21,78] The unpaired spins are mainly from U $5f$ electrons [Fig. 3(b)]. The calculated magnetic moment of U is 1.99 μ_B, compared with the reported value of 1.9 μ_B from a similar DFT + U calculation.[12] The result suggests that the oxidation state of U is 4+ with two unpaired electrons. The equilibrium cell parameter was estimated by fitting the total energy vs. volume curve, as shown in Fig. 4. With the DFT + U calculation, the optimized cell parameter is 5.54 Å [Fig. 4(b)], ~1.0% larger than the observed value of 5.47 Å.[38] Without the Hubbard U term, the calculated cell parameter is 5.41 Å, ~1.0% lower than the observed value [Fig. 4(a)]. Similar results were reported in a previous DFT study of cubic fluorite UO_2.[12] The bulk modulus was calculated by fitting the total energy as a function of volume (Fig. 4) based on the Birch–Murnaghan equation of state.[81] The calculated bulk modulus is 191.6 GPa, in approximate agreement with 207 GPa and 195.4 GPa in a previous experiment[38] and an *ab initio* calculation,[12] respectively. Without the Hubbard U-ramping method, there are slight changes on the density of states, crystal cell parameter, and bulk modulus, as shown in dashed lines in Fig. 3 and Table III. The valence O $2p$ bands in the range of -1.6 to approximately -5.8 eV are shifted to -2.1 to approximately -6.8 eV [Fig. 3(c)] and the bottom of the U $5f$ conduction bands are also shifted to lower energies by 0.3 eV [Fig. 3(b)]. The calculated bulk modulus is 193.4 GPa. Although the Hubbard U-ramping method brings the total

TABLE III. Calculated properties of stoichiometric and hyperstoichiometric uranium dioxide.

	UO_2					$UO_{2.03}$			
	Fluorite structure			Cotunnite structure		Fluorite structure		Cotunnite structure	
Properties	W/o ramping	U-ramping	Exp.	W/o ramping	U-ramping	W/o ramping	U-ramping	W/o ramping	U-ramping
Cell parameter (Å)	5.54	5.54	5.47[38]	5.41*	5.41*	5.53	5.54	5.43*	5.44*
Bulk modulus (GPa)	193.4	191.6	207[38]	151.3	134.5	154.3	176.5	161.8	138.2
Band gap (eV)	1.9	2.2	2.1[77]	2.1	2.1	0	1.3	1.7	1.3

*The cell parameters for the cotunnite structure is calculated with $V^{1/3}$ for comparison.

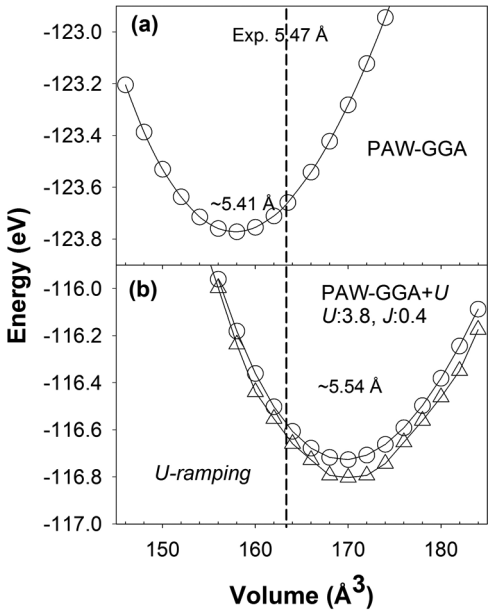

FIG. 4. Total energy as a function of volume of UO_2 with the fluorite structure. The symbols are calculated values and the thin lines are eye guides. The vertical dashed-line is the experimental observed cell volume (Ref. 38). (a) GGA-PAW and spin-polarized calculation without the Hubbard U term. (b) GGA-PAW and spin-polarized calculation with the Hubbard U terms ($U = 3.8$ and $J = 0.4$) without (open circles) and with (open triangles) the Hubbard U-ramping method.

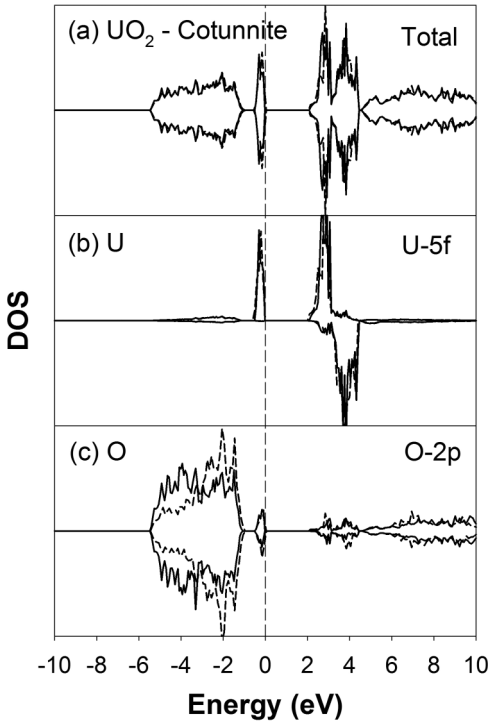

FIG. 5. Electron density of states (DOS) of UO_2 with cotunnite structure with (solid lines) and without (dashed lines) the Hubbard U-ramping method. (a) Total density of states. (b) Partial density of states of an up-spin U atom. (c) Partial density of states of an O atom. The vertical dashed line is the location of the Fermi level. Each DOS is arbitrarily rescaled for clarity.

energy down by ∼0.1 eV/12-atom cell, the electronic and crystal structure are only insignificantly different from the results when no U-ramping is applied.

For stoichiometric UO_2 with orthorhombic cotunnite structure, the band gap width is unknown. Thus, the Hubbard U parameter for the cotunnite structure cannot be estimated, as has been done for the fluorite structure. In order to have a consistent base for the comparison between the two structures, in this study, the same Hubbard U value used for the fluorite structure was chosen for the cotunnite structure. As shown in a previous study,[14] a change of the U parameter will shift the total energy, which will affect the calculated phase transition pressure. Since the primary purpose of this study is to understand the effects of the stoichiometry on the electronic structure and phase transition pressure, the focus is the relative changes of the properties not the absolute values; therefore, the conclusion is not expected to be significantly affected by the choice of the Hubbard U parameter. The magnetic structure of the cotunnite structure is also unknown. In order to check for the ground magnetic structure, calculations were performed with different AFM orderings and ferromagnetic ordering. The AFM ⟨001⟩ order has a slightly higher energy, 2.1 meV/12 atoms higher than the ⟨100⟩ order. The AFM ⟨010⟩ order has a much higher energy, 40.1 meV/12 atoms above the ⟨100⟩ order. The AFM higher orders (e.g., ⟨110⟩ and ⟨111⟩ orders) have higher energies than the AFM ⟨100⟩ order. The ferromagnetic order is 35.3 meV/12 atoms above the ⟨100⟩ order. These results show that the AFM ordered structure with the magnetic moments of U atoms in the ⟨100⟩ directions has the lowest energy. The details of the calculations will be reported separately.

With the ⟨100⟩ AFM and same Hubbard U value as the fluorite structure, the calculated band gap width of the cotunnite structure is ∼2.1 eV (Fig. 5). The densities of states of the U and O atoms [Figs. 5(b) and 5(c)] are similar to those of UO_2 with fluorite structure. The calculated bulk modulus is 134.5 GPa, a 30% decrease compared with UO_2 with the fluorite structure. This result suggests that, for stoichiometric UO_2, in spite of their different structures, the electronic properties are similar for both the cubic and orthorhombic phases. The structural differences, such as the symmetries, bond lengths, and coordination numbers, result in a large difference in bulk modulus. Although the cotunnite phase is denser than the fluorite phase, the ⟨U-O⟩ bond length and coordination number of U in the cotunnite structure are larger than in the fluorite structure. The average ⟨U-O⟩ bond length in the former (∼2.5 Å) is longer than in the latter (∼2.4 Å) at their equilibrium volumes at zero pressure, which leads to a much smaller bulk modulus for the high-pressure phase. A similar relation has been observed experimentally for a defect pyrochlore between its low-pressure fluorite structure and high-pressure cotunnite structure.[82] Without the Hubbard U-ramping method, there are negligible changes on the density of states as shown in Fig. 5.

B. Properties of hyperstoichiometric $UO_{2.03}$

For hyperstoichiometric $UO_{2.03}$ with the fluorite structure, the major change in the density of states for the increased oxygen content is the appearance of new bands at the bottom

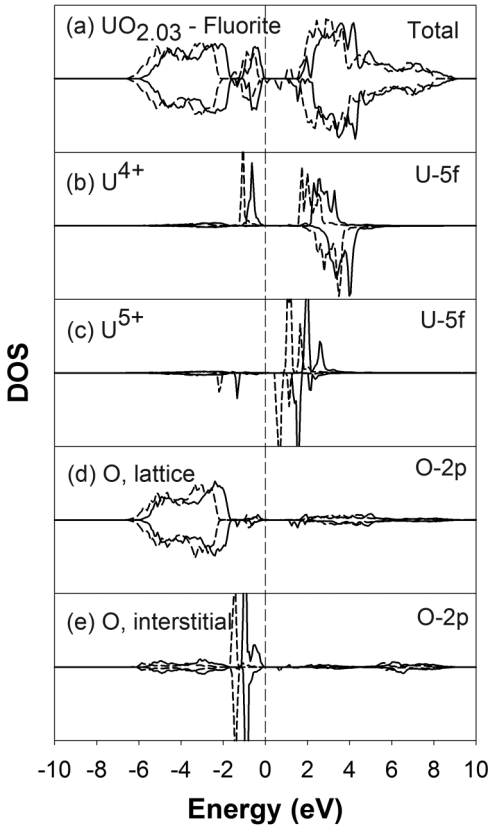

FIG. 6. Electronic density of states (DOS) of hyperstoichiometric $UO_{2.03}$ with the fluorite structure with (solid lines) and without (dashed lines) the Hubbard U-ramping method. (a) The total density of states. (b) Partial density of states of an up-spin U^{4+} atom. (c) Partial density of states of a down-spin U^{5+} atom. (d) Partial density of states of a normal O atom in the lattice. (e) Partial density of states of the interstitial O atom. The vertical dashed line is the location of the Fermi level. Each DOS is arbitrarily rescaled for clarity.

of the conduction band within the band gap of stoichiometric UO_2, as shown in Fig. 6(a). The new bands, mainly $5f$ electrons, are shifted to lower energy [Fig. 6(c)] by ~0.8 eV [Fig. 6(b)], resulting in a band gap of 1.3 eV. The calculated magnetic moment is 1.12 μ_B for the U atoms that also cause the new bands [Fig. 6(c)] and ~1.99 μ_B for the rest of the U atoms. The loss of magnetic moment can be interpreted as an oxidation of that U atom from U^{4+} to U^{5+}. There are two such U^{5+} atoms in the structure. Both of the U^{5+} atoms are three bonds away from the interstitial oxygen. The oxidized U atoms are not necessarily the nearest neighbors of the interstitial oxygen, as shown in previous studies.[10,31] Structures with different locations of the two U^{5+} atoms are expected to have different energies. In this study, for a qualitative understanding of the electronic structure, the lowest energy structure of all possible U^{5+} configurations was not sought, which would be a subject of future studies. For the U atoms that are not oxidized, the density of states of the U [Fig. 6(b)] atoms is similar to that of stoichiometric UO_2 with the cubic structure. The density of states contribution of the interstitial oxygen [Fig. 6(e)] is different from that of the lattice O atoms [Fig. 6(d)]. All the oxygen atoms, including the interstitial O atom, have similar effective charges and negligible magnetic moments. This result suggests that the interstitial O atom receives the two electrons from the two oxidized U atoms (i.e., U^{5+}) three bonds away.

Without using the Hubbard U-ramping method, the main change is that most of the bands are shifted to lower energies [dashed lines, Fig. 6(a)]. For U^{4+} and lattice and interstitial O, the energy shift is ~0.4 eV, and for U^{5+}, the shift is ~0.8 eV. The as-converged structure without the Hubbard U-ramping method also indicates some bands from U^{5+} in the middle of the gap [Fig. 6(a)], which may be caused by the metastability of the system. One of the two U^{5+} atoms is located at the nearest neighbor of the interstitial oxygen, and the other U^{5+} is three bonds away from the interstitial oxygen, different from those using the U-ramping method. These results suggest that the metastability could lead to a different defect band structure.

For hyperstoichiometric $UO_{2.03}$ with orthorhombic cotunnite structure, the band gap is reduced to 1.3 eV [Fig. 7(a)], 0.8 eV smaller than the stoichiometric UO_2 with the same structure. The calculated magnetic moment of U is ~2.0 μ_B, except for two U atoms with a magnetic moment of ~1.2 μ_B, indicating two U^{5+}. The total density of states and the densities of states of all species (Fig. 7) are

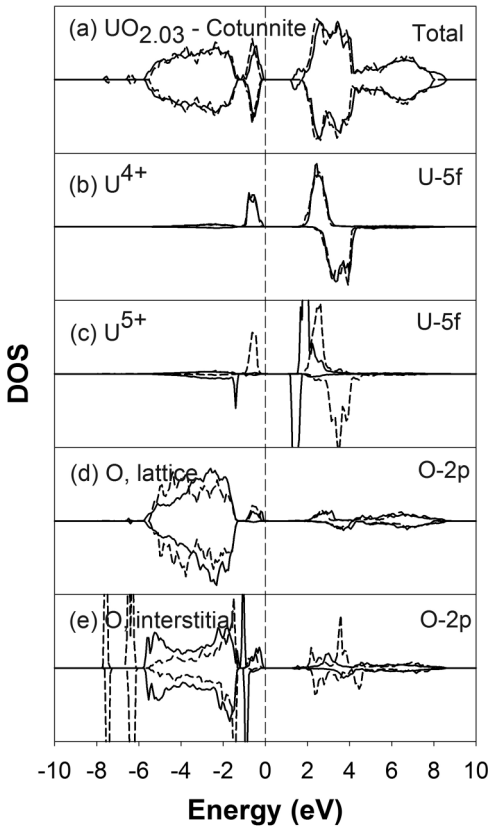

FIG. 7. Electronic density of states (DOS) of $UO_{2.03}$ with the cotunnite structure with (solid lines) and without (dashed lines) the Hubbard U-ramping method. (a) The total density of states. (b) Partial density of states of an up-spin U^{4+} atom. (c) Partial density of states of a down-spin U^{5+} atom with the U-ramping method. Without the U-ramping method, all the U atoms are the same as in panel (c). (d) Partial density of states of a lattice O atom. (e) Partial density of states of the interstitial oxygen atom. The vertical dashed line is the location of the Fermi level. Each DOS is arbitrarily rescaled for clarity.

similar to those of $UO_{2.03}$ with the fluorite structure. The calculated bulk modulus is 138.2 GPa, similar to the stoichiometric UO_2 with the same structure, or a 22% decrease from the fluorite-structure $UO_{2.03}$. Without using the Hubbard U-ramping method, the main difference is that the interstitial oxygen (and one of the lattice O atoms) has new deep bands appearing around -6.4 and -7.4 eV below the Fermi level [Fig. 7(e)]. In contrast to the hyperstoichiometric $UO_{2.03}$ with the cubic fluorite structure, the calculated magnetic moment of U is $\sim 2.0\ \mu_B$ for all U atoms, similar to the stoichiometric UO_2. This result suggests that there is no oxidation state change for any of the U atoms in the system and all the U atoms still have $4+$ oxidation states. Apparently, without using the Hubbard U-ramping method, the system is converged to a different electronic state and defect structure, which will be discussed in the next section.

C. Charge transfer induced by the interstitial oxygen in hyperstoichiometric $UO_{2.03}$

The interstitial O atom introduced into hyperstoichiometric $UO_{2.03}$ interacts with the neighboring atoms and the rest of the system and causes a redistribution of the electron density with respect to stoichiometric UO_2. For hyperstoichiometric $UO_{2.03}$ with the fluorite structure, without using the Hubbard U-ramping method, the charge density around the interstitial oxygen shifts towards one of the six neighboring U atoms [Fig. 8(a)]. This U atom has a magnetic moment of 1.10 μ_B and $5+$ oxidation state. With the Hubbard U-ramping method, the charge density around the interstitial oxygen shifts towards two neighboring U atoms [Fig. 8(b)], and these two U atoms are U^{4+} and two bonds away from the U^{5+} atoms [not showing in Fig. 8(b)]. Note that the average distance between the interstitial oxygen and the neighboring U atoms is 2.77 Å, larger than the distance (2.34 Å) between the lattice oxygen and lattice uranium. The U^{5+} atoms near the interstitial O may be the reason why the center of the U octahedron interstitial site is not the most stable position for the interstitial oxygen. The interstitial oxygen is shifted from the center of the U octahedron by $\sim$0.15 Å in the ⟨100⟩ direction [Fig. 8(a)] and

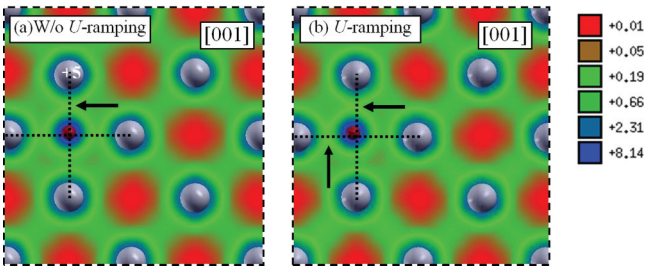

FIG. 8. (Color online) Total charge density maps of hyperstoichiometric $UO_{2.03}$ of the cubic structure without (a) and with (b) the Hubbard U-ramping method. The arrows point to the regions showing the charge density with increased sharing between the interstitial oxygen and neighboring U atoms. The interstitial oxygen (the small ball) moves off center of the U (large balls) octahedron. The dotted lines connect the octahedral U atoms, indicating the center of the U octahedron. Charge density is represented by a (natural) logarithmic scale and the values are in atomic units (e/Å^3).

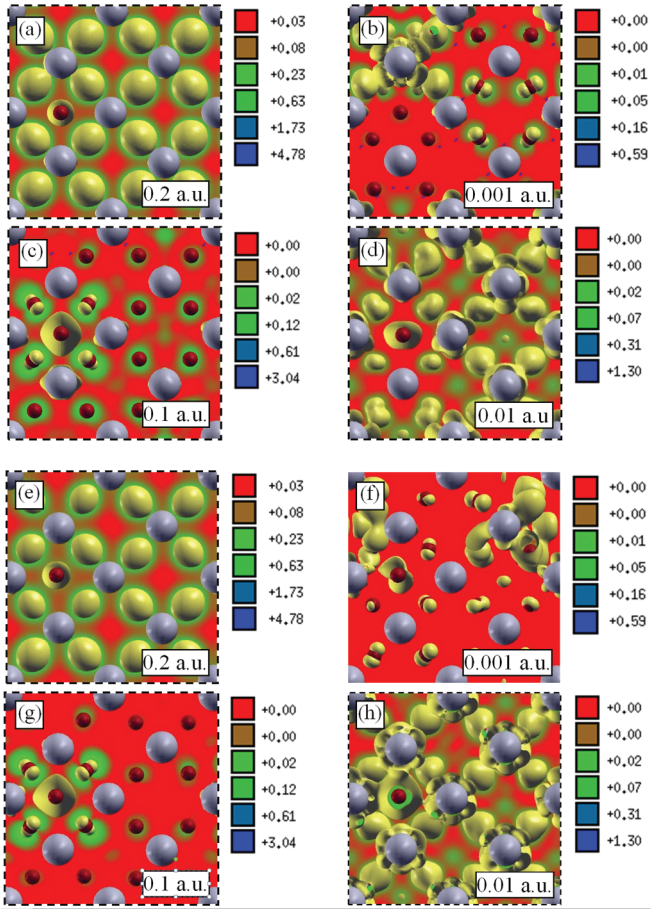

FIG. 9. (Color online) Partial (band-decomposed) charge density map of hyperstoichiometric $UO_{2.03}$ of the cubic structure. Without the Hubbard U-ramping method, the energy ranges of the density maps are $-6.0 \rightarrow -2.4$ eV (a), $-2.4 \rightarrow -2.0$ eV (b), $-1.9 \rightarrow -1.2$ eV (c), and $-1.2 \rightarrow 0.0$ eV (d). With the Hubbard U-ramping method, the energy ranges of the density maps are $-6.0 \rightarrow -2.0$ eV (e), $-1.5 \rightarrow -1.1$ eV (f), $-1.1 \rightarrow -0.8$ eV (g), and $-0.8 \rightarrow 0.0$ eV (h). Isosurfaces (yellow) are plotted along with the charge density and its value is shown in the figure. The density scales are in natural logarithm. The values are in atomic units (e/Å^3).

0.21 Å in the ⟨110⟩ direction [Fig. 8(b)] without and with the U-ramping method, respectively.

The redistribution of the electron density associated with such a shift and oxidation of the U atoms is also reflected in the partial charge density maps (Fig. 9). Without the Hubbard U-ramping method, the charge density map [Fig. 9(a)] for the electron band energies between -6.0 and -2.4 eV shows extended electronic states contributed mainly from O $2p$ (lattice and interstitial) orbitals. For the energy range between -2.4 and -2.0 eV, Fig. 9(b) indicates mostly localized states, mainly from $5f$ orbitals of the oxidized U (e.g., U^{5+}) and its neighboring O $2p$ orbitals, and hybridization between them is also clearly shown, suggesting that the electronic orbitals are also partially delocalized. For energies between -1.9 and -1.2 eV, the map [Fig. 9(c)] suggests localized states associated with the interstitial oxygen, which is extended to the next nearest neighbor oxygen atoms. The extended states involving both the O $2p$ and U $5f$ electrons are also observed in the energy range

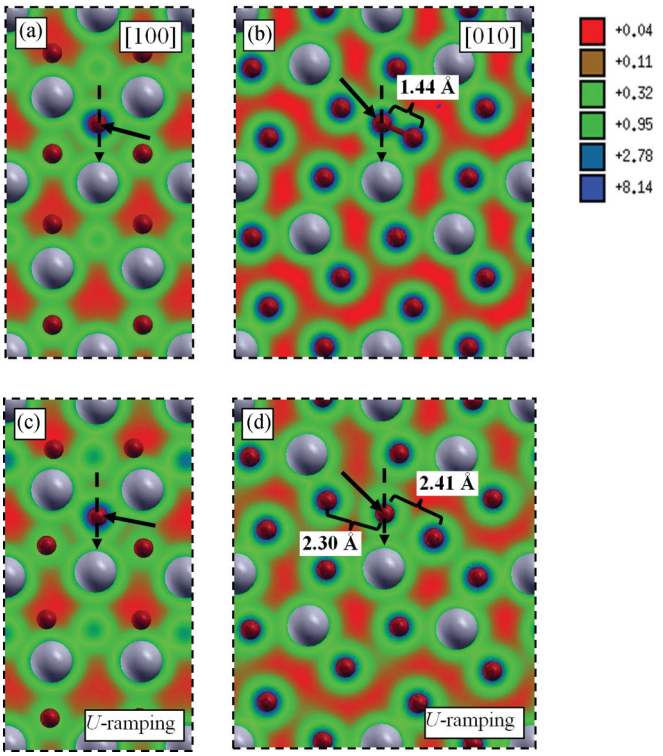

FIG. 10. (Color online) Total charge density maps of hyperstoichiometric $UO_{2.03}$ of the orthorhombic structure projected along [100] and [010] without (a), (b) and with (c), (d) the Hubbard U-ramping method, respectively. The arrows point to the interstitial oxygen atom. The dashed arrow shows the moving direction of the interstitial oxygen. The peroxide unit is shown in panel (b). Charge density is represented by a (natural) logarithmic scale, and the values are in atomic units ($e/Å^3$).

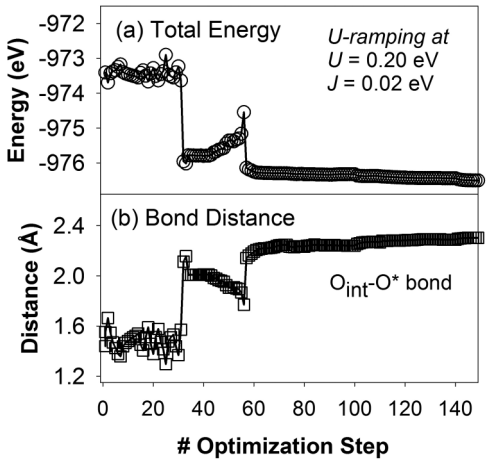

FIG. 11. The total energy (a) and bond distance (b) between the interstitial oxygen and a lattice oxygen as a function of the optimization step of the orthorhombic structure with the U-ramping method at $U = 0.2$ eV. The starting configuration with a peroxide unit is the converged structure without the U-ramping method optimized with $U = 3.8$ eV and $J = 0.4$ eV.

of −1.2 and 0.0 eV, [Fig. 9(d)]. With the Hubbard U-ramping method, the partial charge densities for the energies in all the ranges are similar to those without the Hubbard U-ramping method in comparable energies, as shown in Figs. 9(e)–9(h). These results indicate that the metastability has a noticeable effect on the location of the U^{5+} atoms but has a minor effect on the charge density distribution.

For hyperstoichiometric $UO_{2.03}$ with the cotunnite structure, without the Hubbard U-ramping method, the total charge densities around the U atoms neighboring the interstitial oxygen are similar to the densities of the remaining U atoms. However, as shown in Figs. 10(a) and 10(b), the interstitial O atom migrates about ∼1.0 Å away from its initial position parallel to [001] direction and forms a bond with a lattice oxygen with a bond distance of 1.44 Å [Fig. 10(b)]. Compared with the O-O bond distance of the peroxide unit in studtite ($[(UO_2)(O_2)(H_2O)_2](H_2O)_2$, 1.46 Å),[83] in hydrogen peroxide (H_2O_2, 1.48 Å), in ozone (O_3, 1.23 Å), and in the O_2 molecule (1.21 Å),[84] the O-O bond distance in hyperstoichiometric $UO_{2.03}$ with the cotunnite structure suggests that a peroxide unit with a single bond between the oxygen atoms is formed. The peroxide unit acts as a single charge entity accepting two electrons, one for each of the peroxide O atoms. The rest of the O atoms are unperturbed and similar to those of stoichiometric UO_2. With the Hubbard U-ramping method, the total charge densities [Figs. 10(c) and 10(d)] are similar to those obtained without U-ramping, except that the peroxide unit is not formed. Instead, the distances between the interstitial O and the two nearest O atoms are 2.30 and 2.41 Å, similar to the distance between the interstitial O and the nearest O atoms (i.e., ∼2.44 Å) in $UO_{2.03}$ with the fluorite structure. In order to test whether the peroxide unit is stable, the structure with a peroxide unit, converged from without the U-ramping method, was used as the starting configuration, and the U-ramping method and allowing positions of atoms to relax were then used to ramp up the U parameter. As Fig. 11 shows, the peroxide unit is dissociated during the U-ramping procedure with the U at 0.2 eV. This result suggests that the different optimization procedures could direct the system to go through different paths, leading to different defect structures with different energies. However, the final energy difference between the two defect structures resulting from without and with the U-ramping method is rather small (i.e., ∼0.07 eV/12-atom cell). It would be interesting to find out if the peroxide unit in hyperstoichiometric UO_{2+x} with the cotunnite structure, predicted without using the U-ramping method, can be detected experimentally (e.g., using a spectroscopic method).

Similar to the fluorite structure, partial (band-decomposed) charge density maps for the cotunnite structure are shown in Fig. 12. Without the Hubbard U-ramping method, for the energy range between −8.0 and −7.0 eV, the electronic states are highly localized at the peroxide unit from the peroxide unit [Fig. 12(a)]. Similar electron localization is observed for the energies between −7.0 and −6.0 eV [Fig. 12(b)]. These two bands form a bonding and an anti-bonding state of the O-O single bond with O $2p$ orbital characters in the peroxide unit. States in the energy range between −5.5 and −1.5 eV are associated with O atoms [Fig. 12(c)]. For energies between −1.0 and 0.0 eV [Fig. 12(d)], both U and O atoms contribute to the density. With the Hubbard U-ramping method, the map with the energies between −6.0 and −1.5 eV

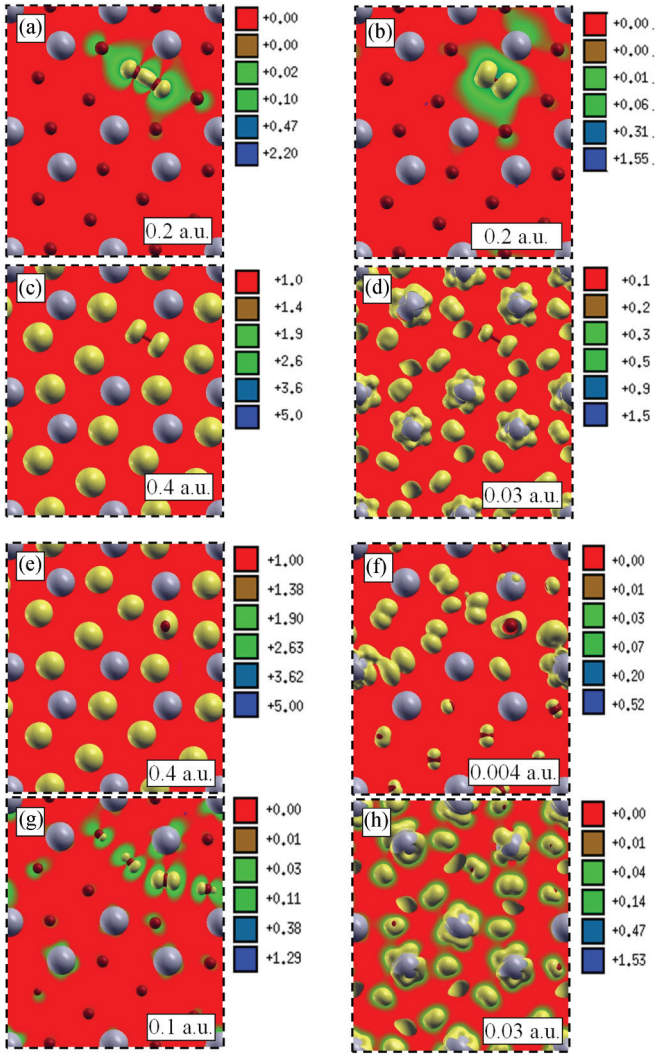

FIG. 12. (Color online) Partial (band-decomposed) charge density map of hyperstoichiometric $UO_{2.03}$ of the orthorhombic structure. Without the Hubbard U-ramping method, the energy ranges of the density maps are $-8.0 \rightarrow -7.0$ eV (a), $-7.0 \rightarrow -6.0$ eV (b), $-5.5 \rightarrow -1.5$ eV (c), and $-1.0 \rightarrow 0.0$ eV (d). With the Hubbard U-ramping method, the energy ranges of the density maps are $-6.0 \rightarrow -1.5$ eV (e), $-1.5 \rightarrow -1.2$ eV (f), $-1.2 \rightarrow -0.8$ eV (g), and $-0.8 \rightarrow 0.0$ eV (h). Isosurfaces (yellow) are plotted along with the charge density, and the values are shown in the figures. The scales for the density are in natural logarithm. The values are in atomic units ($e/Å^3$).

[Fig. 12(e)] is similar to that between -5.5 and -1.5 eV without the Hubbard U-ramping method [Fig. 12(c)], except for the density surrounding the peroxide unit. For the energies between -1.5 and -1.2 eV [Fig. 12(f)], the charge density shows mainly the states from $5f$ of U^{5+} with contributions from O $2p$, similar to that of U^{5+} states of $UO_{2.03}$ with the fluorite structure in the energies between -2.4 and -2.0 eV. For the energies between -1.2 and -0.8 eV [Fig. 12(g)], the charge density is mainly from the interstitial O atom. For the energies between -0.8 and 0.0 eV [Fig. 12(h)], the charge density is mainly from the lattice U^{4+}, with contributions from O $2p$, similar to lattice U^{4+} in $UO_{2.03}$ with the fluorite structure [Fig. 9(h)].

As a result, the calculated charge densities in Figs. 8–10 and 12 show that the defect states in the cubic and orthorhombic structures are both partially localized and partially delocalized around the interstitial oxygen. The local defect structures are similar in both structures. However, without the U-ramping method, the interstitial oxygen atoms in the orthorhombic structure form a peroxide unit with adjacent lattice O atoms, leading to fully localized states around the interstitial oxygen. This result suggests that without the U-ramping method, the calculation could converge the orthorhombic $UO_{2.03}$ to a metastable state with a different defect structure.

D. Phase transitions of UO_2 and $UO_{2.03}$ under pressure

At high pressure, UO_2 undergoes a cubic $Fm\bar{3}m$ to orthorhombic $Pnma$ structural phase transition as observed by experiments.[38,39] In a recent high-pressure and high-temperature experimental study, a cubic modified-fluorite $Pa\bar{3}$ phase and an orthorhombic $Pbca$ phase were observed using a natural UO_2 sample with ~8 wt% of PbO.[54] In that study, the phase transition from the cubic fluorite structure to the orthorhombic cotunnite structure was not detected, probably because of a large number of impurities in the samples and the high temperatures of the experiments. In this paper, the focus is the phase transition from the cubic fluorite structure to the orthorhombic cotunnite structure under pressure as a function of stoichiometry. Theoretically, the phase transition pressure between two phases can be readily estimated by using the following two equivalent approaches. At the transition pressure and assuming equilibrium conditions, the two phases coexist and have the same pressure, $P_f = -dE_f(V_f)/dV_f = P_c = -dE_c(V_c)/dV_c$, and the same enthalpy, $H_f = E_f(V_f) + P^*V_f = H_c = E_c(V_c) + P^*V_c$, where E is the total energy of the system and H the enthalpy, P is the system pressure, and V is the system volume. The subscripts indicate the cubic fluorite (f) phase and orthorhombic cotunnite (c) phase. Therefore, the phase transition pressure can be estimated by the slope of the cotangent of the two-phase curves from a plot of total energy as a function of volume based on the first equation, or by the pressure from the solution of the second equation. At ambient temperature, the vibrational entropic contribution, which is the main contribution to the entropy, to the free energy for oxides is expected to be small. This has been demonstrated for another oxide, TiO_2.[85] Thus, the entropic contribution to the total energy is neglected in this study, and enthalpy is used in place of free energy.

The total energy as a function of volume is plotted for the fluorite and cotunnite phases (Fig. 13). The calculated phase transition pressure from the fluorite structure to the cotunnite structure is significantly affected by a small amount of interstitial oxygen, as the slopes in Fig. 13 show. Without the U-ramping method [Fig. 13(a)], for stoichiometric UO_2, the calculated phase transition pressure is ~17 GPa, in line with the result of ~20 GPa from a similar DFT + U calculation.[12] In contrast, for hyperstoichiometric $UO_{2.03}$, the calculated transition pressure is ~27 GPa, a significant increase (~59%) from that of the stoichiometric UO_2. With the U-ramping method, the results are similar [Fig. 13(b)]. This means that with a small amount of extra oxygen (i.e., 0.2 wt% in this study), the estimated transition pressure is much closer to

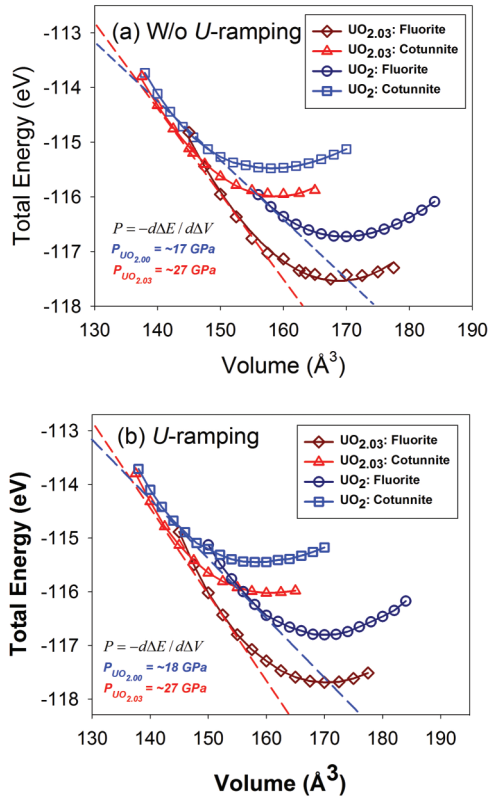

FIG. 13. (Color online) Total energy as a function of system volume without (a) and with (b) the Hubbard U-ramping method. For hyperstoichiometric $UO_{2.03}$ using the 97-atom cell, the volumes and calculated energies are scaled by a factor of one-eighth to be comparable to the cells with 12 atoms. The dashed line is the cotangent of the two curves involving a phase transition. Symbols are calculated values: circles (UO_2-fluorite), squares (UO_2-cotunnite), diamonds ($UO_{2.03}$-fluorite), and triangles ($UO_{2.03}$-cotunnite). The thin lines are eye guides.

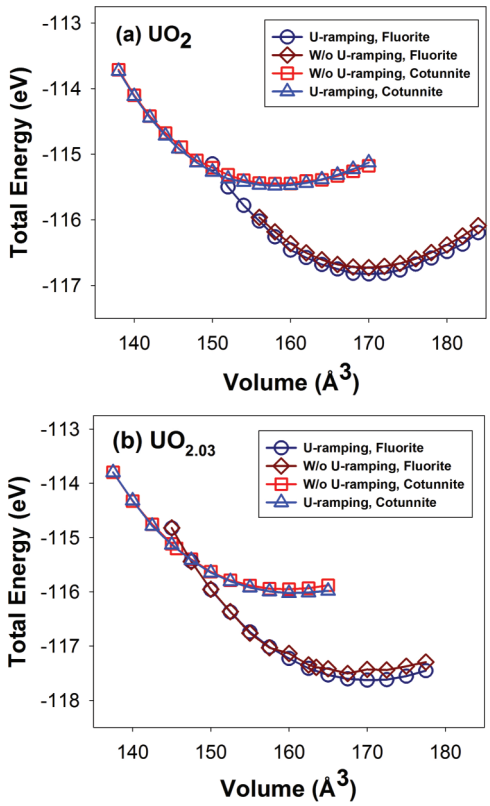

FIG. 14. (Color online) Total energy as a function of system volume without and with the Hubbard U-ramping method for UO_2 (a) and $UO_{2.03}$ (b). The effect of the U-ramping method on the calculated energy appears clearly.

the experimentally observed transition pressures of 29 GPa[39] and 42 GPa.[38] It is unknown if the samples used in these experiments are ideal stoichiometric UO_2. For natural UO_2 samples, a large deviation from the ideal chemical composition leads to a different phase transition behavior under pressure, as demonstrated in a recent experimental high-pressure study.[54] However, the details of the stoichiometry (i.e., oxygen content) of the samples were not provided in that study.[54] As shown in Fig. 13, the increase of the estimated transition pressure is mainly caused by a difference in the energy changes near their equilibrium volumes between UO_2 and $UO_{2.03}$ for the two phases. For the fluorite structure, the energy difference is -0.9 eV from UO_2 to $UO_{2.03}$, and -0.6 eV for the cotunnite structure [Fig. 13(b)]. For the hyperstoichiometric $UO_{2.03}$ calculations, metastable electronic states of $UO_{2.03}$ affect the calculated energies, as indicated by a deviation of the calculated data points from the parabolic curves near the equilibrium volumes [Fig. 13(a)] without the U-ramping method. The deviation is more pronounced for the fluorite phase than for the cotunnite phase.

As discussed in the methods section and shown in Fig. 13, the electronic metastability causes an error on the calculated energies, which could potentially affect the accuracy of the calculated phase transition pressures (e.g., the slopes of the cotangents). In order to clearly show the magnitude of energy differences, Fig. 14 plots together the total energy as a function of volume with and without the U-ramping method for UO_2 [Fig. 14(a)] and $UO_{2.03}$ [Fig. 14(b)]. As shown, the largest difference is near the equilibrium volume. Without the U-ramping method, the as-converged states of UO_2 are 0.08 and 0.04 eV/12-atom cell above the ground state for the cubic and orthorhombic structures, respectively, and 0.16 and 0.07 eV/12-atom cell for $UO_{2.03}$ for the two structures, respectively. Although metastability has a noticeable effect on the ground state energies, it has a negligible effect on the calculated phase transition pressure. The reason is that the magnitude of the errors (i.e., $\sim$0.1 eV) is rather small with respect to the energy difference between the two structures (i.e., $\sim$1 eV) and that the errors are partially canceled out in the calculated energy difference between the two structures, leading to an even smaller error in the calculated phase transition pressure.

The calculated volume as a function of pressure, which can be readily determined experimentally, is plotted in Fig. 15. Without the U-ramping method [Fig. 15(a)], at low pressures for both the fluorite and cotunnite structures, the volumes of hyperstoichiometric $UO_{2.03}$ are less than for stoichiometric UO_2, in line with the results that show that the incorporation of excess oxygen into UO_2 reduces the volume of the cubic fluorite phase without using any of the methods to remove metastable states.[21,72] At high pressures (>5 GPa), the inter-

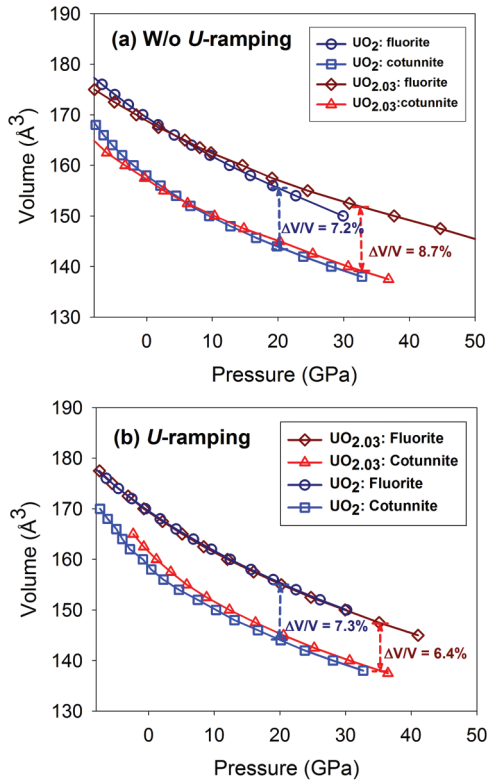

FIG. 15. (Color online) Volume as a function of pressure values without (a) and with (b) the Hubbard U-ramping method. Symbols are calculated. Thin lines are eye guides. The vertical dashed lines with arrows show the volume changes of the phase transitions at the transition pressures.

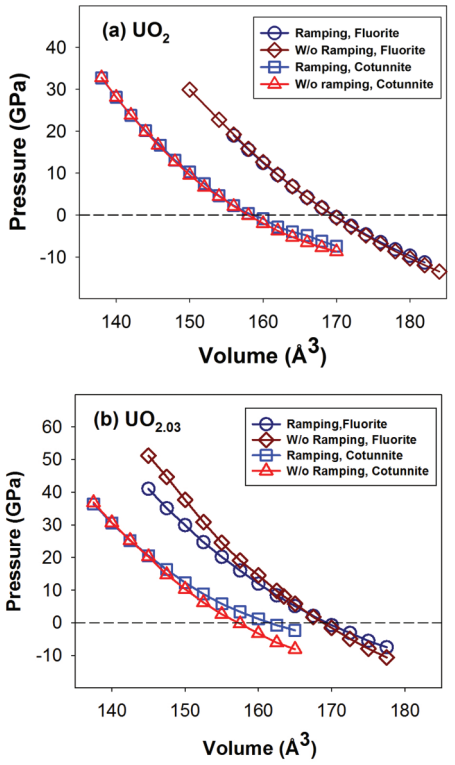

FIG. 16. (Color online) Volume as a function of pressure without and with the Hubbard U-ramping method for UO_2 (a) and $UO_{2.03}$ (b). The effect of the U-ramping method on the calculated volume appears clearly.

stitial oxygen increases the volumes for both the cubic and orthorhombic structures of hyperstoichiometric $UO_{2.03}$ with respect to stoichiometric UO_2. The volume change for the phase transition at the transition pressure (∼17 GPa) is 7.2% for UO_2, compared with an earlier theoretical calculation of 7.3% without any of the methods to remove the metastable state.[12] For $UO_{2.03}$, the volume change is 8.7% at ∼27 GPa. With the U-ramping method [Fig. 15(b)], the calculated volume change at the phase transition pressures are 7.3% and 6.4% for UO_2 and $UO_{2.03}$, respectively, in agreement with an experimental value of 7%.[38] The U-ramping method leads to a smaller volume change for $UO_{2.03}$ and a similar change for UO_2, compared with volume changes without the U-ramping method. For the fluorite structure, the volumes of both compositions are similar over the pressures studied. For the cotunnite structure, $UO_{2.03}$ has a larger volume than UO_2, caused by the interstitial oxygen.

In order to clearly show the effect of metastability on the calculated volume, Fig. 16 plots together the calculated pressure as a function of volume with and without the U-ramping method for UO_2 [Fig. 16(a)] and $UO_{2.03}$ [Fig. 16(b)]. For UO_2, the volumes are almost identical for both structures in the pressure range studied. The equilibrium volumes are also similar with and without the U-ramping method. For $UO_{2.03}$, the U-ramping method predicts a less steep pressure vs. volume curve for both structures. For the fluorite structure, the calculated equilibrium volumes are similar with and without the U-ramping method. For the cotunnite structure, the calculated equilibrium volume is larger with the U-ramping method compared with that without the U-ramping method. This is because the interstitial oxygen forms a peroxide bond with a lattice oxygen without the U-ramping method but stays as an interstitial using the U-ramping method.

E. Effect of interstitial oxygen on the electronic and structural properties of $UO_{2.03}$

The dramatic effect of interstitial oxygen on the phase transition pressure indicates a fundamental difference in the way in which the interstitial oxygen is incorporated into the fluorite and cotunnite structures. In terms of electronic structure, for the fluorite structure, the electronic states associated with the defect are partially localized and partially delocalized, as evident from the charge transfer to interstitial oxygen from two U atoms three bonds away. In addition, new bands appear at the top of the band gap of UO_2, which mainly originate from the $5f$ electrons of the oxidized U^{5+} atoms. For the cotunnite structure, the electronic states are also partially localized and partially delocalized, similar to those of the fluorite structure. The charge transfer to the interstitial oxygen is similar to that of the fluorite structure. It is interesting to observe that, without the U-ramping method to remove metastable states, the calculation predicts localizations of the electronic states associated with the interstitial oxygen, as evident from the formation of a peroxide unit (interstitial O and one lattice O) and the more or less unperturbed density of states and charge density of the rest of the system.

In terms of the local structure around the interstitial oxygen atom, the cubic fluorite structure provides a vacancy, the so-called octahedral interstitial site. Incorporating an O atom into this position is energetically favorable[21] and does not cause the system volume to increase.[72] In contrast, the high-pressure phase with the cotunnite structure is denser and more compact with respect to the low-pressure phase. The structure does not have a site where the interstitial oxygen can be easily located, resulting in an increase of the calculated volumes [Table III, Fig. 15(b)].

The energy of incorporating an interstitial O atom into the cubic or orthorhombic structure provides a measure on how difficult it is for the structure to accommodate an excess oxygen atom. The difference in energies between the two structures, which can be readily obtained from Fig. 13(b), shows that, at ambient pressure, the cotunnite structure requires 0.3 eV more energy to incorporate the interstitial oxygen than does the fluorite structure. At 10 GPa, the incorporation energy difference increases to 0.5 eV, indicating that it is even more difficult to incorporate the interstitial oxygen into the orthorhombic structure as pressure increases. As shown in Fig. 13(b), the energy difference results in a significant increase of the phase transition pressure for hyperstoichiometric $UO_{2.03}$. The effect of the interstitial oxygen is also reflected in the calculated bulk modulus of each phase (Table III). Comparing the bulk modulus of $UO_{2.03}$ with UO_2, the bulk modulus of the fluorite structure is reduced by 8% to 176.5 GPa from 191.6 GPa, but that of the cotunnite structure is increased by 3% to 138.2 GPa from 134.5 GPa.

IV. CONCLUDING REMARKS

One of the unique features of the cubic fluorite structure of UO_{2+x} is that it can have a range of stoichiometries depending on the temperature and oxygen pressure. Although variations in the oxygen diffusivity of UO_2 have long been documented,[33,52,86] the effect on other properties of fundamental interest, such as the phase transition pressure as investigated in this study, has not previously been explored. The present results show an unexpected effect of the interstitial oxygen on the phase transition pressure between the cubic and orthorhombic phases. As the x value of UO_{2+x} increases from 0.00 to 0.03, the calculated phase transition pressure from the fluorite structure to the cotunnite structure increases from 18 to 27 GPa, an ∼50% increase. These findings can be tested by systematic experimental studies of the pressure-induced phase transition as a function of composition. In addition, these calculations reveal interesting electronic structures of UO_{2+x} upon incorporation of the excess oxygen. The details of the effects, including the defect bands, defect structure, charge transfer, and oxidation of uranium from $4+$ to $5+$ in both of the structures, can be tested by experimental techniques including spectroscopic methods. The electronic metastability of UO_2 using the DFT + U method, as demonstrated in the recent literature, indeed causes errors in the calculated properties, such as density of states, electron density, defect structure, equilibrium volume, and phase transition pressure. Although the metastability could lead to a state for which its energy is as high as 0.16 eV/12-atom cell above the ground state, in many cases, the errors of the calculated properties are small. For instance, the effect on the calculated phase transition pressure between the fluorite and cotunnite phases is negligible. One exception is that metastability could lead to a completely different defect structure in the orthorhombic phase, where a peroxide unit is formed between interstitial oxygen and lattice oxygen. These results suggest that the electronic metastability of UO_2 needs to be carefully checked for stoichiometric or nonstoichiometric systems, or systems with defects, if the DFT + U method is used.

ACKNOWLEDGMENTS

This work was supported by the *Center for the Materials Science of Actinides*, an Energy Frontier Research Center, funded by the US Department of Energy, Office of Basic Energy Sciences (DE-SC0001089). We used the National Energy Research Scientific Computing Center (NERSC), which is supported by the Office of Science of the US Department of Energy under Contract No. DE-AC02-05CH11231. Computational resources were made available in part by the National Science Foundation through XSEDE resources from NCSA and NICS under Grants No. TG-DMR080047N and No. TG-DMR100034.

*Mailing address: Department of Earth and Environmental Sciences 1100 North University Avenue, 2534 C.C. Little Building, Ann Arbor, Michigan 48109-1005, USA; jwwang@umich.edu; current address: Department of Geology & Geophysics, Louisiana State University, E235 Howe-Russell, Baton Rouge, LA 70803, USA; jianwei@lsu.edu

[1] J. Janeczek, R. C. Ewing, V. M. Oversby, and L. O. Werme, J. Nucl. Mater. **238**, 121 (1996).

[2] P. C. Burns, R. C. Ewing, and A. Navrotsky, Science **335**, 1184 (2012).

[3] R. L. Williamson, J. D. Hales, S. R. Novascone, M. R. Tonks, D. R. Gaston, C. J. Permann, D. Andrs, and R. C. Martineau, J. Nucl. Mater. **423**, 149 (2012).

[4] M. Stan, Nucl. Eng. Technol. **41**, 39 (2009).

[5] M. Stan, J. C. Ramirez, P. Cristea, S. Y. Hu, C. Deo, B. P. Uberuaga, S. Srivilliputhur, S. P. Rudin, and J. M. Wills, J. Alloys Compd. **444**, 415 (2007).

[6] B. J. Lewis, W. T. Thompson, F. Akbari, D. M. Thompson, C. Thurgood, and J. Higgs, J. Nucl. Mater. **328**, 180 (2004).

[7] H. Matzke and M. Kinoshita, J. Nucl. Mater. **247**, 108 (1997).

[8] D. A. Andersson, B. P. Uberuaga, P. V. Nerikar, C. Unal, and C. R. Stanek, Phys. Rev. B **84**, 054105 (2011).

[9] J.-P. Crocombette, D. Torumba, and A. Chartier, Phys. Rev. B **83**, 184107 (2011).

[10] F. N. Skomurski, J. W. Wang, R. C. Ewing, and U. Becker, J. Nucl. Mater. **434**, 422 (2013).

[11]R. Devanathan, L. Van Brutzel, A. Chartier, C. Gueneau, A. E. Mattsson, V. Tikare, T. Bartel, T. Besmann, M. Stan, and P. Van Uffelen, Energy Environ. Sci. **3**, 1406 (2010).
[12]J. G. Yu, R. Devanathan, and W. J. Weber, J. Phys.: Condens. Matter **21**, 435401 (2009).
[13]B. Dorado, B. Amadon, M. Freyss, and M. Bertolus, Phys. Rev. B **79**, 235125 (2009).
[14]H. Y. Geng, Y. Chen, Y. Kaneta, and M. Kinoshita, Phys. Rev. B **75**, 054111 (2007).
[15]I. D. Prodan, G. E. Scuseria, and R. L. Martin, Phys. Rev. B **76**, 033101 (2007).
[16]J. E. Klepeis, J. Mater. Res. **21**, 2979 (2006).
[17]K. N. Kudin, G. E. Scuseria, and R. L. Martin, Phys. Rev. Lett. **89**, 266402 (2002).
[18]S. L. Dudarev, D. N. Manh, and A. P. Sutton, Philos. Mag. B **75**, 613 (1997).
[19]V. A. Gubanov, A. Rosen, and D. E. Ellis, Solid State Commun. **22**, 219 (1977).
[20]B. Dorado, G. Jomard, M. Freyss, and M. Bertolus, Phys. Rev. B **82**, 035114 (2010).
[21]P. Nerikar, T. Watanabe, J. S. Tulenko, S. R. Phillpot, and S. B. Sinnott, J. Nucl. Mater. **384**, 61 (2009).
[22]H. Y. Geng, Y. Chen, Y. Kaneta, M. Iwasawa, T. Ohnuma, and M. Kinoshita, Phys. Rev. B **77**, 104120 (2008).
[23]F. Gupta, G. Brillant, and A. Pasturel, Philos. Mag. **87**, 2561 (2007).
[24]M. Iwasawa, Y. Chen, Y. Kaneta, T. Ohnuma, H. Y. Geng, and M. Kinoshita, Mater. Trans. **47**, 2651 (2006).
[25]J. P. Crocombette, F. Jollet, L. N. Nga, and T. Petit, Phys. Rev. B **64**, 104107 (2001).
[26]E. D. A. Ferriss, R. C. Ewing, and U. Becker, Am. Mineral. **95**, 229 (2010).
[27]T. Watanabe, S. B. Sinnott, J. S. Tulenko, R. W. Grimes, P. K. Schelling, and S. R. Phillpot, J. Nucl. Mater. **375**, 388 (2008).
[28]C. B. Basak, A. K. Sengupta, and H. S. Kamath, J. Alloys Compd. **360**, 210 (2003).
[29]P. J. D. Lindan and M. J. Gillan, J. Phys.: Condens. Matter **3**, 3929 (1991).
[30]J. Wang and U. Becker, J. Nucl. Mater. **433**, 424 (2013).
[31]B. Dorado, P. Garcia, G. E. L. Carlot, C. Davoisne, M. Fraczkiewicz, B. Pasquet, M. Freyss, C. Valot, G. Baldinozzi, D. Siméone, and M. Bertolus, Phys. Rev. B **83**, 035126 (2011).
[32]F. Gupta, A. Pasturel, and G. Brillant, Phys. Rev. B **81**, 014110 (2010).
[33]D. A. Andersson, T. Watanabe, C. Deo, and B. P. Uberuaga, Phys. Rev. B **80**, 060101 (2009).
[34]Y. Yun, P. M. Oppeneer, H. Kim, and K. Park, Acta Mater. **57**, 1655 (2009).
[35]B. Meredig, A. Thompson, H. A. Hansen, C. Wolverton, and A. van de Walle, Phys. Rev. B **82**, 195128 (2010).
[36]H. Y. Geng, Y. Chen, Y. Kaneta, M. Kinoshita, and Q. Wu, Phys. Rev. B **82**, 094106 (2010).
[37]F. Jollet, G. Jomard, B. Amadon, J. P. Crocombette, and D. Torumba, Phys. Rev. B **80**, 235109 (2009).
[38]M. Idiri, T. Le Bihan, S. Heathman, and J. Rebizant, Phys. Rev. B **70**, 014113 (2004).
[39]U. Benedict, G. D. Andreetti, J. M. Fournier, and A. Waintal, J. Phys. Lett. **43**, L171 (1982).
[40]B. Amadon, F. Jollet, and M. Torrent, Phys. Rev. B **77**, 155104 (2008).
[41]G. Jomard, B. Amadon, F. Bottin, and M. Torrent, Phys. Rev. B **78**, 075125 (2008).
[42]F. Tran, J. Schweifer, P. Blaha, K. Schwarz, and P. Novak, Phys. Rev. B **77**, 085123 (2008).
[43]W. T. Thompson, B. J. Lewis, E. C. Corcoran, M. H. Kaye, S. J. White, F. Akbari, Z. He, R. Verrall, J. D. Higgs, D. M. Thompson, T. M. Besmann, and S. C. Vogel, Int. J. Mater. Res. **98**, 1004 (2007).
[44]C. Gueneau, M. Baichi, D. Labroche, C. Chatillon, and B. Sundman, J. Nucl. Mater. **304**, 161 (2002).
[45]P. Y. Chevalier, E. Fischer, and B. Cheynet, J. Nucl. Mater. **303**, 1 (2002).
[46]Y. Saito, J. Nucl. Mater. **51**, 112 (1974).
[47]K. Une and M. Oguma, J. Nucl. Mater. **115**, 84 (1983).
[48]T. L. Markin, V. J. Wheeler, and R. J. Bones, J. Inorg. Nucl. Chem. **30**, 807 (1968).
[49]K. Hagemark and M. Broli, J. Inorg. Nucl. Chem. **28**, 2837 (1966).
[50]J. Belle, J. Nucl. Mater. **30**, 3 (1969).
[51]H. Matzke, J. Nucl. Mater. **30**, 26 (1969).
[52]P. Contamin, J. J. Bacmann, and J. F. Marin, J. Nucl. Mater. **42**, 54 (1972).
[53]H. Matzke, J. Less-Common Met. **121**, 537 (1986).
[54]S. Greaux, L. Gautron, D. Andrault, N. Bolfan-Casanova, N. Guignot, and J. Haines, Am. Mineral. **93**, 1090 (2008).
[55]G. Kresse and J. Furthmuller, *Vienna Ab-initio Simulation Package* (Universität Wien, 2004), http://www.vasp.at/.
[56]P. E. Blöchl, Phys. Rev. B **50**, 17953 (1994).
[57]J. P. Perdew and Y. Wang, Phys. Rev. B **45**, 13244 (1992).
[58]J. P. Perdew, J. A. Chevary, S. H. Vosko, K. A. Jackson, M. R. Pederson, D. J. Singh, and C. Fiolhais, Phys. Rev. B **46**, 6671 (1992).
[59]J. P. Perdew and Y. Wang, Phys. Rev. B **33**, 8800 (1986).
[60]S. L. Dudarev, G. A. Botton, S. Y. Savrasov, C. J. Humphreys, and A. P. Sutton, Phys. Rev. B **57**, 1505 (1998).
[61]J. Hafner, J. Comput. Chem. **29**, 2044 (2008).
[62]J. Hafner, Comput. Phys. Commun. **177**, 6 (2007).
[63]P. Santini, S. Carretta, G. Amoretti, R. Caciuffo, N. Magnani, and G. H. Lander, Rev. Mod. Phys. **81**, 807 (2009).
[64]R. Laskowski, G. K. H. Madsen, P. Blaha, and K. Schwarz, Phys. Rev. B **69**, 140408 (2004).
[65]J. C. Boettger and A. K. Ray, Int. J. Quantum Chem. **80**, 824 (2000).
[66]J. C. Boettger and A. K. Ray, Int. J. Quantum Chem. **90**, 1470 (2002).
[67]I. D. Prodan, G. E. Scuseria, J. A. Sordo, K. N. Kudin, and R. L. Martin, J. Chem. Phys. **123**, 014703 (2005).
[68]I. D. Prodan, G. E. Scuseria, and R. L. Martin, Phys. Rev. B **73**, 045104 (2006).
[69]L. E. Roy, R. L. Martin, T. Durakiewicz, J. J. Joyce, and G. Scuseria, in *ADTSC Science Highlights 2008*, edited by Susanne King and Kathy Pallis (Los Alamos National Laboratory, Los Alamos, NM, 2008), p. 98.
[70]P. Zhang, B.-T. Wang, and X.-G. Zhao, Phys. Rev. B **82**, 144110 (2010).
[71]B. T. M. Willis, Acta Crystallogr. Sect. A **34**, 88 (1978).
[72]L. Desgranges, M. Gramond, C. Petot, G. Petot-Ervas, P. Ruello, and B. Saadi, J. Eur. Ceram. Soc. **25**, 2683 (2005).
[73]H. Y. Geng, Y. Chen, Y. Kaneta, and M. Kinoshita, Phys. Rev. B **77**, 180101 (2008).
[74]E. Yakub, C. Ronchi, and D. Staicu, J. Nucl. Mater. **389**, 119 (2009).

[75] A. I. Liechtenstein, V. I. Anisimov, and J. Zaanen, Phys. Rev. B **52**, R5467 (1995).
[76] Y. Baer and J. Schoenes, Solid State Commun. **33**, 885 (1980).
[77] J. Schoenes, J. Appl. Phys. **49**, 1463 (1978).
[78] D. Gryaznov, E. Heifets, and E. Kotomin, Phys. Chem. Chem. Phys. **11**, 7241 (2009).
[79] L. Petit, A. Svane, Z. Szotek, W. M. Temmerman, and G. M. Stocks, Phys. Rev. B **81**, 045108 (2010).
[80] L. E. Cox, W. P. Ellis, R. D. Cowan, J. W. Allen, S. J. Oh, I. Lindau, B. B. Pate, and A. J. Arko, Phys. Rev. B **35**, 5761 (1987).
[81] F. Birch, Phys. Rev. **71**, 809 (1947).
[82] F. X. Zhang, M. Lang, U. Becker, R. C. Ewing, and J. Lian, Appl. Phys. Lett. **92**, 011909 (2008).
[83] P. C. Burns and K.-A. Hughes, Am. Mineral. **88**, 1165 (2003).
[84] E. A. Dawi, A. M. Vredenberg, G. Rizza, and M. Toulemonde, Nanotechnology **22**, 215607 (2011).
[85] J. He, R. K. Behera, M. W. Finnis, X. Li, E. C. Dickey, S. R. Phillpot, and S. B. Sinnott, Acta Mater. **55**, 4325 (2007).
[86] J. F. Marin and P. Contamin, J. Nucl. Mater. **30**, 16 (1969).